Variational and diffusion Monte Carlo techniques for quantum clusters

R. N. Barnett and K. B. Whaley
Department of Chemistry, University of California, Berkeley, California 94720
(Received 21 August 1991; revised manuscript received 18 November 1992)

The H_2-^{4}He dimer and small ^{4}He clusters are studied using Monte Carlo sampling techniques. We consider alternative wave-function forms in order to obtain high accuracy efficiently. For the smaller systems, both guided and unguided Metropolis walks are used and the effciencies are studied. Of particular concern is accurate sampling at small particle separations and the behavior of the local energy in this regime. As a final step, we compute exact energies by a diffusion Monte Carlo method. We obtain converged energies significantly below the Green's-function Monte Carlo values, which employed an earlier He-He potential with a slightly shallower well. For He_3 and He_{20}, the Green's-function Monte Carlo energies are reproduced when employing the same potential. However, for the 112-atom cluster, our converged energy lies below the Green's-function Monte Carlo value. Second-order estimates of the exact density profiles and particle separation distributions, p, are also determined. For the 14- and 20-atom clusters, second-order estimates of p show enhanced structure in comparison to variational Monte Carlo results. Statistically meaningful oscillations in the second-order estimates of the exact density profiles are not observed.

PACS number(s): 36.40.+d, 67.40.Db, 02.70.−c, 03.65.Ge

I. INTRODUCTION

Atomic and molecular clusters have become of interest to both theorists and experimentalists [1]. Of particular concern are structure, phase transitions, binding energies, and excitation spectra, and the behavior of these properties as the bulk is approached.

We are interested in studying atomic and molecular clusters, both pure and with impurities attached, using Monte Carlo techniques. Such approaches thus far possess the greatest possibility of yielding high accuracy for theoretical methods. To enhance the capabilities of Monte Carlo for these systems, we consider alternative wave-function forms and the efficient optimization of wave-function parameters in studying weakly bound quantum clusters. To start with, we study the H_2He complex (from here on ^{4}He is assumed). This system is quite useful as it provides a very weakly bound, highly repulsive potential, test case for the initial wave-function form we employ.

As a further development, we employ diffusion Monte Carlo (DMC). We use this approach to compute exact ground-state energies for helium clusters with the most up-to-date potential. In addition to increased accuracy in the energy and structural features such as the density profile, the DMC approach serves to provide benchmarks for evaluating wave-function quality. This is pertinent for the helium clusters for which exact energies resulting from the most recent pair potential have not yet been computed.

The remainder of the paper is organized as follows. In Sec. II we discuss Monte Carlo integration techniques, and in Sec. III the exact diffusion Monte Carlo approach. The wave-function forms and optimization technique we employ are presented in Sec. IV. In Sec. V we present results for a range of small clusters ($N \leq 20$ and $N = 112$). Section VI presents conclusions concerning the wave-function accuracy and sampling efficiency for all techniques.

II. MONTE CARLO INTEGRATION TECHNIQUES

Multidimensional integration is performed by Monte Carlo in order to obtain wave-function expectation values. This is achieved by sampling points, $\mathbf{R}=(\mathbf{r}_1,\mathbf{r}_2,\ldots,\mathbf{r}_N)$, from a probability density function $p(\mathbf{R})$. Expectation values of coordinate operators $A(\mathbf{R})$ are then computed as

$$\overline{A}_M \equiv M^{-1}\sum_{i=1}^{M} A(\mathbf{R}_i) , \tag{1}$$

with $\{\mathbf{R}_i\}$ sampled from p. As M becomes large, $\overline{A}_M$ approaches the average of $A(\mathbf{R})$ over $p(\mathbf{R})$.

We employ two variants of the Metropolis walk [2,3] to sample p. The first of these is the widely used and very simple "unguided" walk. For a point at $\mathbf{R}$, a new point is sampled from a transition probability density $T(\mathbf{R}\rightarrow\mathbf{R}')$ which is simply constant within a cube and zero outside. Thus moves are given by

$$\mathbf{R}'=\mathbf{R}+\Delta(\xi-0.51) , \tag{2}$$

where ξ is a vector whose components are uniform random variates between 0 and 1.

This "unguided" walk attempts to move uniformly through coordinate space without regard to the form of $|\Psi|^2$. Therefore a more efficient scheme of choosing attempted moves is likely. This is the basis of a guided or "smart" Metropolis walk, which is also known as importance sampling. We now choose the transition density to be

$$T(\mathbf{R}\rightarrow\mathbf{R}')=(4\pi\Delta)^{-3N/2}\exp\{-[\mathbf{R}'-\mathbf{R}-\Delta\mathbf{F}(\mathbf{R})]^2/4\Delta\} . \quad (3)$$

Sampling from this transition density requires that

$$\mathbf{R}'=\mathbf{R}+\Delta\mathbf{F}(\mathbf{R})+\sqrt{2\Delta}\chi . \quad (4)$$

The components of χ are Gaussian random numbers with a mean of zero and a variance of unity, which we obtain by the Box-Mueller algorithm [4]. The "guiding force," $\mathbf{F}=\nabla|\Psi|^2$, acts to push moves in the direction of most rapidly increasing $|\Psi|^2$.

The major consideration for the approaches discussed here is the value of Δ which yields the most efficient sampling. The optimum choice lies between a small value, which yields a high acceptance rate but a large degree of correlation between moves, and a large value, which gives large attempted displacements but a very small acceptance rate so that correlation is large. The optimum Δ is often taken to be that which yields an average acceptance rate (or ratio) of roughly 0.5. Here we consider a further quantitative measurement of the efficiency with which configuration space is sampled, namely, the average displacement of moves during the walk, $\langle\Delta R\rangle$. (A rejected move contributes a value of zero to this average.)

III. DIFFUSION MONTE CARLO

Although the Metropolis algorithm provides a means for computing expectation values of a given wave function, accuracy is limited by the quality of Ψ. However, exact Monte Carlo approaches are well known. These approaches are often generically referred to as quantum Monte Carlo and fall into two categories, Green's-function Monte Carlo (GFMC) and diffusion Monte Carlo. The former has been applied to a wide range of problems and derives from consideration of the time-independent Schrödinger equation. Initial work was on the helium atom [5] and liquid helium [6,7], and later applications include electronic structure calculations [8,9] and computations on helium clusters [10–12].

DMC starts with the time-dependent Schrödinger equation in imaginary time and has been employed mostly in electronic structure calculations [13–17]. Recent work has also included helium clusters and other van der Waals species [18–20]. The DMC approach we employ is very similar to that of Reynolds *et al.* [15] and is outlined below.

Writing the Schrödinger equation in imaginary time, $t\rightarrow t/i$, and setting $\hbar=1$ we have

$$-\frac{\partial\Phi(\mathbf{R},t)}{\partial t}=(H-E_R)\Phi(\mathbf{R},t) . \quad (5)$$

The reference energy E_R only affects the (imaginary) time dependence of $\Phi(\mathbf{R},t)$. It is easily shown that at large t the ground state dominates, leaving

$$\Phi=\exp[-t(E_0-E_R)]\phi_0 . \quad (6)$$

Note that the choice of $E_R\approx E_0$ is useful in removing the time dependence from the asymptotic solution.

Importance sampling is implemented by choosing a probability density function $f\equiv\Psi\Phi$, where Ψ is a trial wave function. Rewriting Eq. (5) in terms of f gives

$$-\frac{\partial f}{\partial t}=-D\nabla^2 f+D\nabla\cdot[f\mathbf{F}(\mathbf{R})]+[E_L(\mathbf{R})-E_R]f , \quad (7)$$

where

$$H=-D\nabla^2+V, \quad D\nabla^2\equiv\sum_i(2m_i)^{-1}\nabla_i^2 ,$$

$E_L\equiv\Psi^{-1}H\Psi$ is the local energy, and once again $\mathbf{F}\equiv\nabla\ln|\Psi|^2$. Note that terms on the right-hand side of Eq. (7) correspond to diffusion, drift, and branching, respectively. The asymptotic form of f follows from Eq. (6) and is

$$f(\mathbf{R},t)=\exp[-t(E_0-E_R)]\Psi(\mathbf{R})\phi_0(\mathbf{R}) . \quad (8)$$

When f takes this form, expectation values over f are independent of t, i.e.,

$$\langle A\rangle_f\equiv\int f(\mathbf{R},t)A(\mathbf{R})d\mathbf{R}\Big/\int f(\mathbf{R},t)d\mathbf{R}$$
$$=\int\Psi(\mathbf{R})\phi_0(\mathbf{R})A(\mathbf{R})d\mathbf{R}\Big/\int\Psi(\mathbf{R})\phi_0(\mathbf{R})d\mathbf{R} .$$

For $A(\mathbf{R})=E_L(\mathbf{R})$, it is easily shown that $\langle E_L\rangle_f=E_0$, so that the ground-state energy is obtained as the average of E_L over f. The time development of f is given by

$$f(\mathbf{R}',t+\tau)=\int d\mathbf{R}\,f(\mathbf{R},t)G(\mathbf{R}\rightarrow\mathbf{R}',\tau) , \quad (9)$$

where the Green's function G describes a move from $\mathbf{R}$ to $\mathbf{R}'$ in time τ. The Green's function is a solution of Eq. (7) with the boundary condition $G(\mathbf{R}\rightarrow\mathbf{R}',0)=\delta(\mathbf{R}-\mathbf{R}')$. For all but a few simple Hamiltonians, the Green's function is unknown. Here, we employ an analytic "short-time" approximation to G which takes the form

$$G_a(\mathbf{R}\rightarrow\mathbf{R}',\tau)=(4\pi D\tau)^{-3N/2}$$
$$\times\exp\{-[\mathbf{R}'-\mathbf{R}-D\tau\mathbf{F}(\mathbf{R})]^2/4D\tau\}$$
$$\times\exp(-\tau\{[E_L(\mathbf{R}')+E_L(\mathbf{R})]/2-E_R\}) . \quad (10)$$

The approximate nature of G_a is clear from Eq. (10): during the course of a move from $\mathbf{R}$ to $\mathbf{R}'$ in time τ, the drift [determined by $\mathbf{F}(\mathbf{R})$] and branching (dependent on E_L) are assumed to be constant. While error in G_a vanishes as $\tau\rightarrow 0$ [21–23], for the practical case, i.e., $\tau\neq 0$, the asymptotic f only approximates $\Psi\phi_0$, and computed results will differ from the corresponding averages over $\Psi\phi_0$. This difference, referred to as time-step bias, may either be removed by extrapolation or made insignificant by using values of τ such that the bias is less than the statistical error.

To reduce time-step bias, an acceptance-or-rejection step is employed [15]. That is, moves are accepted with a probability A given by

$$A(\mathbf{R}\rightarrow\mathbf{R}',\tau)=\min\{1,w(\mathbf{R}\rightarrow\mathbf{R}',\tau)\} , \quad (11)$$

and

$$w(\mathbf{R}\rightarrow\mathbf{R}',\tau)=\frac{|\Psi(\mathbf{R}')^2|G_a(\mathbf{R}'\rightarrow\mathbf{R},\tau)}{|\Psi(\mathbf{R})|^2G_a(\mathbf{R}\rightarrow\mathbf{R}',\tau)} . \quad (12)$$

Including the factor A plays an important role. As Ψ approaches the exact solution ϕ_0, the branching becomes constant and G_a is essentially the transition density given in Eq. (3) with $\Delta=D\tau$. In this instance, DMC reduces to a guided Metropolis walk and $f(=|\phi_0|^2)$ is sampled without time-step bias—for any value of τ. Use of A has been found to greatly reduce time-step bias [24] because the acceptance-or-rejection step eliminates time-step bias to the extent that Ψ resembles ϕ_0.

We conclude this section with a discussion of several technical details. In the DMC [and Metropolis-walk or variational Monte Carlo (VMC)] computations, ten independent ensembles of 100 walkers are propagated in parallel yielding ten independent estimates, of, for example, the energy, from which the average and its statistical error are obtained. If greater precision is desired, more runs are performed in this manner. This structure is useful in that for each set of runs an estimate of statistical error unbiased by serial correlation is computed.

Updating the reference energy E_R is useful for minimizing the time dependence of the ensemble. For a given number [or population, $P(0)$] of points sampled from $f(0)=\Psi\phi_0$ at the beginning of the DMC walk, we have

$$P(0)=\int f(\mathbf{R},0)d\mathbf{R} \ . \tag{13}$$

From the asymptotic form of f it is easily seen that

$$P(t)=\exp[-t(E_0-E_R)]P(0) \ . \tag{14}$$

Note that Eq. (14) indicates that an estimate of E_0 may be obtained from the change in the ensemble size over time. This estimate, usually referred to as the growth energy (E_G), often possesses a different dependence on the time step than does the average of the local energy E_L. Therefore, to reduce the long-term growth or decay of ensemble size, at each time step we perform a short run to estimate E_G and then set E_R equal to this estimate when computing the reported results.

Another point concerns the renormalization of the ensemble population P. Even when E_R is equal to the growth estimate of E_0, fluctuations in P arise from fluctuations in E_G, which are in turn caused by variations in the local energy, as the ensemble is propagated. If the statistical error in E_G over the ensemble is σ_{E_G}, then from Eq. (14) the relative statistical error in P is seen to increase proportionally to time as

$$\sigma_P/P=t\sigma_{E_G} \ . \tag{15}$$

Therefore, in keeping the ensemble size reasonable, it is useful to renormalize the population [back to P_0 ($=100$)] at intervals during the walk. However, as noted previously [25], renormalization introduces an error which decreases as the frequency of renormalization decreases. (Generally, this error is not noticeable unless the propagation time between renormalizations is very short.) Here, we divide each run into blocks, and at the end of each block the population is renormalized to 100 walkers. We vary block propagation times (10^4–10^6 hartree^{-1}) to verify that "renormalization" bias is negligible.

The final point concerns the implementation of branching. As seen from Eq. (10), the branching factor for a move from $\mathbf{R}$ to $\mathbf{R}'$ is

$$b(\mathbf{R},\mathbf{R}')=\exp(-\tau\{[E_L(\mathbf{R}')+E_L(\mathbf{R})]/2-E_R\}) \ . \tag{16}$$

Branching may be implemented by obtaining an integer $M=\text{int}[b(\mathbf{R},\mathbf{R}')+\xi]$, where int($x$) is the largest integer that is $\leq x$ and where ξ is a uniform random variate uniformly distributed between 0 and 1 so that $M=b$ on average, and creating M copies of walkers at $\mathbf{R}'$. Alternatively, one may assign a weight $w(\mathbf{R}')=b(\mathbf{R},\mathbf{R}')w(\mathbf{R})$ to the walker at $\mathbf{R}'$. Since M equals b only on average, assigning (or carrying) weights would seem preferable. However, carried weights diverge towards 0 or ∞ as the walk proceeds, giving rise to the possibility that an ensemble may be effectively composed of a few walkers with very large relative weights. In this event, the sampling is inefficient as only a few of the many walkers being propagated contribute to the computed averages. Therefore we employ a combination of carrying weights and copying. Weights are carried unless $w\leq w_{\min}$ or $w\geq w_{\max}$. If either of the bounds are exceeded then $M_w=\text{int}(w+\xi)$ copies are made, and for $w\geq w_{\max}$ each copy is assigned a weight of w/M_w. For the DMC results reported here, $w_{\min}=0.1$–0.4 and $w_{\max}=2$.

IV. TRIAL FUNCTION FORM AND OPTIMIZATION

A. Trial functions

We seek ground-state wave functions for bosonic systems. Such wave functions are nodeless and therefore may be taken as everywhere positive. A convenient representation takes the form

$$\Psi(\mathbf{R})=\exp\left[\sum_I T_I(\mathbf{R})\right] \ , \tag{17}$$

where in the completely general case

$$T_I(\mathbf{R})=\sum_{\substack{i,j,k,\ldots \\ (i<j<k<\cdots)}} t_I(\mathbf{r}_i,\mathbf{r}_j,\mathbf{r}_k,\ldots) \ . \tag{18}$$

In practice I is taken to be ≤ 3 so that the wave function is reasonably compact. Since the potential is given by the sum of pairwise interactions, we omit T_1 and instead start with two-body terms. (One-body terms have been employed in previous studies of clusters [10,26,27], but are not necessary.) We then add on three-body terms for increased accuracy if desired. This reflects the fact that two-body effects should be most important, especially for weakly bound clusters, followed by three-body effects, etc.

As is common practice, we employ a two-body term which is a function only of particle separations, i.e.,

$$T_2(\mathbf{R})=\sum_{\substack{i,j \\ (i<j)}} t_2(\mathbf{r}_i,\mathbf{r}_j)=\sum_{\substack{i,j \\ (i<j)}} t_2(r_{ij}) \ . \tag{19}$$

This term is both translationally and rotationally invariant, i.e., $\mathbf{P}_{\text{c.m.}}T_2=0$ and $\mathbf{L}T_2=0$, as required for the ground-state wave function. Given the importance of two-body effects, it is useful to explore optimal forms for

t_2. In this vein, H_2He, the first "cluster" in the H_2He_N series, provides an excellent test case as a weakly bound species with an interaction potential very similar to that of He-He. Therefore a form of t_2 which accurately describes H_2He may prove advantageous for the helium clusters as well.

The initial form of t_2 is motivated by our studies of H_2He. For the interaction potential, we use a Lennard-Jones plus van der Waals fit [28] to the *ab initio* data of V_0 computed by Meyer, Hariharan, and Kutzelnigg [29]. Since our potential is a function only of the He distance from the H_2 center of mass, the Schrödinger equation for this system can now be reduced to a one-dimensional problem. A numerical solution for the ground state, $\phi_0^{(N)}$, is obtained with the finite difference algorithm of Schatz [30]. The next step consists of considering forms for Ψ and fitting them to $\phi_0^{(N)}$. The accuracy of both the wave-function fit and the computed energy expectation value allow an assessment of the quality of Ψ.

In determining a useful analytic form for Ψ, we treat the long- and short-range behaviors separately. That is, Ψ takes the form

$$\Psi(r)=\Psi_s(r)\Psi_l(r) , \tag{20}$$

where s and l denote the short- and long-range functions, respectively. The short-range form is chosen to be constant at large r. Given the form of V at small r, a natural choice for Ψ_s is

$$\Psi_s(r)=\exp[P(u)], \quad u=r^{-1} ,$$
$$P(u)=\sum_{k=0}^{5} a_k u^k . \tag{21}$$

The bound on the powers included in P results from the desire to limit singularities in the kinetic energy to be no greater than r^{-12}, given that this is the dominant singularity in our potential [28]. A high-quality form of Ψ_l was found to be

$$\Psi_l=r^b\exp[ar^\alpha] . \tag{22}$$

Since Ψ_s is very nearly constant at large r, we first fit Ψ_l to $\ln[\phi_0^{(N)}]$ in this domain to determine a, b, and α. We then determine the short-range parameters $\{a_k\}$ by fitting in the highly repulsive and in the well regions. The range of points included in the short- and long-range fits determines the parameters, which are listed in Table I. We find that the analytic wave function Ψ is nearly indiscernible from the numerical solution $\phi_0^{(N)}$, and the energy is reproduced to high accuracy, $-0.024\,43$ versus $-0.024\,61$ K—an error of only 0.7%.

TABLE I. Wave-function parameters.

Parameter \ Cluster	H_2He	He_{14}	He_{20}	$He_{112}(T_2)$	$He_{112}(T_2+T_3)$
a	−0.007 315 22	−0.107 061	−0.062	−0.010 00	−0.014 00
b	−1.438 143	−1.046 66	−1.055	−0.850 00	−0.855 0
α	1.138 39	0.559 995	0.545	0.545 031	0.545 031
a_0	0.153 6	−1.323 61	−1.308 01	−1.308 01	−1.308 01
a_1	−14.042 55	−30.193 5	−38.864 6	−38.864 6	−38.864 6
a_2	121.496 28	199.831	310.061	310.061	310.061
a_3	−710.897 88	−845.506	−1370.01	−1370.01	−1370.01
a_4	1726.975 6	1808.98	2484.45	2484.45	2484.45
a_5	−7454.421 4	−4354.11	−3674.60	−3674.60	−3674.60
λ_0		0.012	0.012		0.009
ω_0		1.60	1.60		1.8
r_0		5.0	5.0		4.5
λ_1		0.043	0.043		0.031
ω_1		2.025	2.025		2.225
r_1		3.225	3.225		3.225

Parameter \ Cluster	He_3	He_7	He_{20}
a_0	−3.231 950 0	−3.247 39	−3.413 98
a_1	−0.068 458 3	−0.046 985 0	−0.019 168 9
a_v	8.55	8.65	9.20
α_v	0.840 075 0	0.914 958	0.873 622
β_v	0.086 148 1	0.069 567 6	0.069 104 0
t_0	−682.979	−682.409	−675.000
t_1	588.918	590.085	590.085
t_2	−205.068	−203.773	−203.775
t_3	34.132 1	33.170 9	33.163 3
t_4	−2.628 22	−2.466 31	−2.485 77
t_5	0.060 120 2	0.053 350 9	0.058 852 4

The H_2He wave function gives a two-body function,

$$t_2(r)=b\ln r+ar^{\alpha}+\sum_{k=0}^{5}a_k u^k\ , \tag{23}$$

which we have employed in VMC computations of helium clusters with and without a H_2 impurity [28]. The form of t_2 is structurally similar to forms used previously [10,26,27]. The differences are that in the short-range form *all* powers of r^{-1} up to five are included here, and there is an added flexibility in the long-range form, introduced by the exponent α. As discussed above, the short-range component of t_2 is based on our H_2-He potential which takes a Lennard-Jones form at small separations [28]. While the shape of this potential is similar to that of He-He [31], the analytic forms are quite different. Therefore it is of interest to consider entirely new forms for t_2 based on the short-range behavior of the He-He potential. We employ here the most recent HFD-B(HE) potential of Aziz, McCourt, and Wong [31] for all calculations unless it is explicitly stated that the earlier HFDHE2 [32] potential is used.

We give special emphasis to regions of small separation because the local energy generally possesses its greatest fluctuations as r becomes small. Therefore a two-body form which is more physically correct in this domain will reduce fluctuations in E_L, yielding greater precision, and hopefully greater accuracy, in computed energies. Our new t_2 takes the form

$$t_2'(r)=T(r)v(r)+a_0+a_1r+\gamma\ln r\ , \tag{24}$$

where

$$v(r)=a_v\exp(-\alpha_v r-\beta_v r^2) \tag{25}$$

mimics the short-range form of the He-He potential [31], and

$$T(r)=\sum_{k=0}^{n_k}t_k r^k\ , \tag{26}$$

with $n_k=5$. We have chosen $\gamma=0$ leaving only a singularity of r^{-1} in E_L, arising from the kinetic energy. Other permissible values are $\gamma<\frac{1}{2}$ which give an r^{-2} singularity but a finite statistical error in E_L. With $\gamma=0$, t_0a_v negative and large gives a wave function which is very small but remains nonzero at $r=0$. This reflects the fact that the potential converges to a very large but finite value at $r=0$.

Overall, in comparison to Eq. (23), t_2' gives added emphasis to domains containing small particle separations and somewhat less emphasis to large r. It is hoped that, by directly including a "potential-like" function in Ψ, the highly repulsive potential term will be better canceled by the kinetic contribution, producing smaller fluctuations in E_L at small values of r.

The use of a three-body term in ground-state wave functions has yielded significant improvements in descriptions of both the liquid [33–37] and clusters [10]. Here, we employ the description of three-body correlations used previously in microscopic studies of quantum clusters [10,26,27,38], namely,

$$T_3(\mathbf{R})=\lambda_0\sum_i\left[\Gamma_0^2(i)-\sum_{j\ (\neq i)}\xi_0^2(r_{ij})\right]+\lambda_1\sum_i\left[|\mathbf{\Gamma}_1(i)|^2-\sum_{j\ (\neq i)}\xi_1^2(r_{ij})r_{ij}^2\right]\ , \tag{27}$$

with

$$\mathbf{\Gamma}_l(i)=\sum_{j\ (\neq i)}\xi_l(r_{ij})\mathbf{r}_{ij}^l,\quad l=0,1\ . \tag{28}$$

In Eqs. (27) and (28), we have

$$\xi_0(r)=(r-r_0)\exp\left[-\left[\frac{r-r_0}{w_0}\right]^2\right],\qquad \xi_1(r)=\exp\left[-\left[\frac{r-r_1}{w_1}\right]^2\right]. \tag{29}$$

Derivatives of T_3 are evaluated analytically. This is actually faster than finite difference because derivatives by finite difference require three evaluations of the exponentials in Eqs. (29) while analytic computation requires only one. Overall, adding T_3 to T_2 only increased computation time by about 85% for the 14-, 20-, and 112-atom clusters.

B. Optimization

Wave-function parameters are optimized by hand and by conjugate-gradient line minimization. Although crude, varying parameters by hand is quite useful in complementing more sophisticated techniques. Since initial wave-function parameters are often quite poor, hand optimization can quickly yield large improvements. The resulting wave function can then be used as input for the more sophisticated optimization techniques.

The conjugate-gradient technique [39] seeks a local minimum by moving in directions in parameter space which are conjugate to each other, leading to efficient convergence. Essentially, the algorithm consists of successive line minimizations in parameter space. This procedure requires the computation of the quantity being minimized and of its first derivatives with respect to the wave-function parameters. Here, we consider

$$s^2=\frac{\langle\Psi|[E_L-E_g]^2|\Psi\rangle}{\langle\Psi|\Psi\rangle}\ . \tag{30}$$

This quantity is useful in that one may seek either a minimum in the energy by choosing $E_g\ll\langle E_L\rangle$ or in the variance by choosing $E_g=\langle E_L\rangle$. In the first case, minimizing the energy yields global accuracy, and, in the second, minimizing fluctuations in the local energy emphasizes local accuracy in Ψ. Since computed energies are most often compared in discussions of accuracy, we focus on minimizing the energy.

The integrations in Eq. (30) are performed by averaging over a fixed set of points sampled from a distribution $|\Psi_0|^2$ corresponding to an initial set of parameters [40]. Therefore we minimize the estimate of s^2 given by

$$s_M^2=\frac{\sum_{i=1}^{M}[E_L(\mathbf{R}_i)-E_g]^2|\Psi(\mathbf{R}_i)/|\Psi_0(\mathbf{R}_i)|^2}{\sum_{i=1}^{M}|\Psi(\mathbf{R}_i)/|\Psi_0(\mathbf{R}_i)|^2}\ . \quad (31)$$

The major consideration for the stability and accuracy of the optimization is that s_M^2 accurately approximate s^2. For this reason the ratio $|\Psi/\Psi_0|^2$ is included, reflecting the fact that Ψ changes as parameters are varied, although this requires computing parameter derivatives of Ψ. To enhance numerical precision, we adjust the normalization of Ψ so that $\sum_i|\Psi/\Psi_0|^2=M$. This is useful for clusters with more than five atoms where changes in wave-function parameters have a large effect on the normalization of Ψ, because of its product form, and could make $|\Psi/\Psi_0|^2$ uniformly exceedingly large or small. The remaining determinant of the accuracy of s_M^2 is the number of points in the fixed sample. While a large number of points is desired for high accuracy, M is limited by considerations of computational cost and memory requirements. M is chosen so that the statistical error in the average of E_L over the points is significantly less than the desired improvement in the energy. We have employed 1000–2000 points for the smaller clusters, $He_{3-5,7}$, and 5000 points for He_{14} and He_{20}.

The final step in obtaining reliable optimizations involves updating the fixed sample. As the wave function changes, the points sampled from $|\Psi_0|^2$ become a poorer choice for computing expectation values with respect to $|\Psi|^2$. This is most noticeable when Ψ_0 is of poor quality and Ψ changes significantly during optimization. One manifestation of this degradation of the fixed sample is divergence of the energy to unrealistically low values. Therefore we have found it useful to update the sample by using a Metropolis walk to generate a new set of points sampled from the current wave function (which then plays the role of Ψ_0.) Updating is implemented after the energy has converged or when it begins to diverge.

While the conjugate-gradient technique has been successful for the 3–20-atom clusters, it appears to be much less practical for larger clusters. (For He_{112} we started with the optimized He_{20} parameters and only reoptimized the long-range parameters by hand.) As the number of atoms in the cluster increases, the dimensionality of configuration space which must be represented by the fixed sample of points increases. Therefore larger samples are generally required for the larger clusters.

V. RESULTS AND DISCUSSION

A. Metropolis walks

As discussed in Sec. II, wave-function expectation values may be computed by the Metropolis approach. We first consider H_2He. Since the wave function depends only on the distance of He from the midpoint of H_2, r, the walk takes place in only three dimensions, $\mathbf{r}$.

We start with the unguided walk employing several values of Δ in the range 11–40 Å and $M\approx5\times10^7$. We find that sampling $|\Psi|^2$ for such a diffuse system is not trivial. The energy is reproduced reasonably well, the computed value is generally within one or two standard deviations of the analytic, and the average error is 0.1%. However, we find sizable errors in $\langle r\rangle$ and $r_{\rm rms}=(\langle r^2\rangle)^{1/2}$. The smallest value of Δ produces errors of 6% and 7% in $\langle r\rangle$ and $r_{\rm rms}$, respectively. Apparently, poor efficiency in sampling $|\Psi|^2$ occurs in this case. Upon increasing Δ to 27 Å, giving an acceptance ratio close to the often assumed optimum of 0.5, errors in $\langle r\rangle$ and $r_{\rm rms}$ are reduced to 1% and 2%, respectively. Interestingly, we find that only at a large value of Δ, 40 Å, and a relatively small acceptance ratio of 0.35, is accuracy in $\langle r\rangle$ and $r_{\rm rms}$ comparable to that of the energy, i.e., $\approx0.1\%$.

The average displacement of the moves, $\langle\Delta R\rangle$, sheds light on this behavior. We find that $\langle\Delta R\rangle$ monotonically increases from 2.4 Å at $\Delta=11$ Å to 4.7 Å at $\Delta=40$ Å, correlating with the monotonic increase in the quality of $\langle r\rangle$ and $r_{\rm rms}$. The fact that the local energy is relatively constant at large r, so that the computed energies are only weakly dependent on the accuracy of the sampling in this domain, readily explains the difference in behavior of the energy versus the coordinate expectation values.

As a precursor to DMC, we also performed guided-walk calculations with $\Delta=D\tau$ and $\mathbf{F}=\nabla\ln|\Psi|^2$. Note that T in Eq. (3) is now equivalent to G_a, Eq. (10), if the branching is omitted. We now encountered difficulty in sampling this distribution because of the sharp cutoff at small r. In computing at $\tau=5\times10^4$, 10×10^4, and 20×10^4 hartree^{-1}, we found large errors in the energy, 1% for the first two time steps and 5% for the last, despite the large number of points sampled, $M=(3-6)\times10^7$. The behavior of the computed values of $\langle r\rangle$ and $r_{\rm rms}$ is, however, much different. Good accuracy and precision are obtained for these quantities at $\tau=10\times10^4$ and 20×10^4 hartree^{-1}.

The reason for the poor estimates of the energy is that walkers are either trapped at smaller separations or else they do not sample these domains. This trapping is caused by the guiding force $\mathbf{F}$ being excessively large at small r, where it is proportional to r^{-6}, giving acceptance probabilities practically equal to zero. This in turn yields a poor representation of the density at small r which does affect the computed energy because of the large magnitude of E_L there. This is much less significant for r and r^2 which are relatively small near the origin. Since the effect of $\mathbf{F}$ on the acceptance probability is removed exponentially fast as $\tau\rightarrow0$, the small-r domain is more accurately sampled as τ is reduced. However, efficiency is reduced at small τ because the small average step size gives a larger degree of correlation between moves.

We now consider the pure helium clusters. These systems possess a highly repulsive potential as does H_2He but are more tightly bound. (For example, the binding energy of He_3 is five times greater than that of H_2He.) This causes the computation of expectation values by an unguided walk to be less difficult than for H_2He, presumably because sampling a slowly decaying distribution at large r is no longer required. Despite sampling fewer points in calculations on $He_{3-5,7}$ [$M=(2-6)\times10^6$ versus 5×10^7 for H_2He], for each cluster we observe excellent

agreement between computed expectation values over a range of Δ. For example, with $2.6 < \Delta < 13.2$ Å for He_4, the maximum difference in $\langle r \rangle$ (the average particle separation) is only 0.15% and that in the energy is only 0.07%.

While computed averages do not vary significantly as Δ is changed, statistical error in coordinate expectation values, $\langle r \rangle$ and $R_{\rm rms}$ [$R_{\rm rms}=(\langle R^2 \rangle/N)^{1/2}$, where $R^2=\sum_{i=1}^{N}(\mathbf{r}_i-\mathbf{R}_{\rm c.m.})^2$], decreases as Δ (and $\langle \Delta R \rangle$) increases. In going from the smallest to the largest values of Δ, statistical error in $R_{\rm rms}$ and $\langle r \rangle$ is continuously reduced down to a factor of 2 or more, resulting in a fourfold or greater increase in computational efficiency for these quantities. For the energy, small values of Δ result in low efficiency. However, once Δ, and thereby $\langle \Delta R \rangle$, is of reasonable size, statistical error in the energy is no longer decreased as Δ is increased.

Overall, we find the average displacement $\langle \Delta R \rangle$ to be a useful measurement of the sampling efficiency in that larger values tend to give smaller statistical errors, most noticeably for $R_{\rm rms}$ and $\langle r \rangle$. We point out here that the sampling required to obtain $\langle \Delta R \rangle$ to high precision is quite small. Therefore finding the value of Δ which yields the greatest average displacement may be accomplished with very little computation. Finally, as was the case with H_2He, the acceptance ratios corresponding to the largest $\langle \Delta R \rangle$ were less than 0.5, i.e., 0.38 for He_4 and 0.40 for He_7.

We now turn to the guided walk, which encounters difficulty when sampling at small r for H_2He and does not, therefore, appear useful for helium clusters. However, since the DMC walk we employ consists of the guided walk described above with branching, evaluating the practicality of this guided walk is important in ascertaining the feasibility of our DMC approach for obtaining exact results.

As discussed in Sec. IV, acceptance probabilities in the guided walk globally increase as the time step is reduced. If a time step can be found which is small enough to remove trapping at small r, so that convergence in sampling $|\Psi|^2$ can be obtained, without excessively degrading sampling efficiency, DMC may be practical for helium (and other) quantum clusters. Therefore we now determine values of τ which yield high accuracy in the guided walk for He_{3-5}.

Table II presents guided-walk energies and statistical errors (per point sampled) for He_{3-5} at several values of τ. The effect of trapping is immediately evident from the data in Table II. At the larger time steps the energies are of poor quality. In these walks we have observed that atoms which are too close together do not move during the entire course of a run. (Trapping is found by recording the number of accepted moves for each particle.) As the time step is reduced, particles are no longer trapped throughout the run. The result is a noticeable (and for He_5 a dramatic) improvement in the energy. Finally, we see that at sufficiently small time steps, guided-walk energies are in excellent agreement with those computed by the unguided approach.

The small-r behavior of the sampling, and its dependence on τ, is illustrated in Fig. 1. This figure compares

TABLE II. Guided-walk results for He_{3-5}. Time steps are given in hartree^{-1}, lengths are in Å, and energies are in K.

$10^{-4}\tau$	$\langle \Delta R \rangle$	E/N	$\sigma(E/N)$
		He_3	
25.00	2.14	−0.036 9(33)	7.4
12.50	1.60	−0.036 7(27)	6.0
5.00	1.09	−0.038 1(14)	3.1
2.50	0.80	−0.039 7(16)	5.1
1.25	0.58	−0.041 8(7)	4.4
0.75	0.45	−0.041 41(12)	1.1
Unguided	2.78	−0.041 47(7)	0.14
		He_4	
25.00	1.86	−0.126 9(26)	7.4
15.00	1.55	−0.128 8(6)	2.1
10.00	1.34	−0.128 1(3)	1.1
5.00	1.04	−0.132 9(23)	9.2
2.50	0.78	−0.136 3(19)	10.7
1.25	0.57	−0.136 1(7)	4.4
Unguided	2.21	−0.135 6(1)	0.2
		He_5	
10.00	1.17	−0.34(10)	200
5.00	0.96	−0.34(10)	200
2.00	0.69	−0.248 7(12)	3.4
1.00	0.51	−0.250 17(63)	2.2
0.50	0.37	−0.250 48(51)	2.5
Unguided	1.65	−0.250 23(13)	0.3

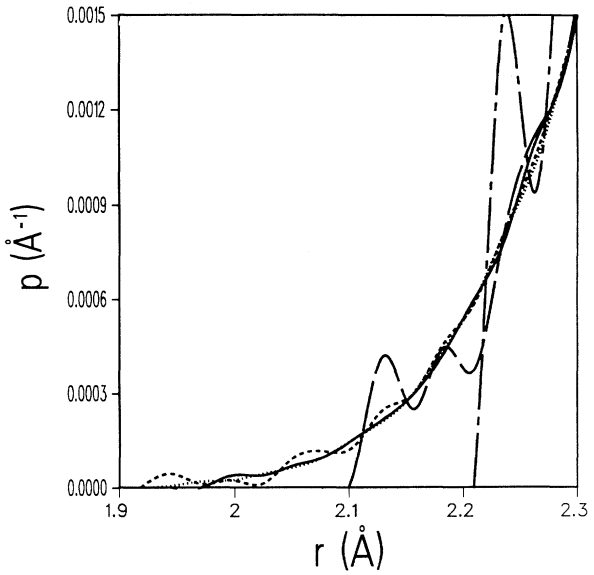

FIG. 1. Convergence of $p(r)$ at small r in the guided walk for He_3. The solid line (——) is the unguided walk, the chain-dashed line (—·—·-) is the guided walk at $\tau=50\,000$ hartree^{-1}, the long-dashed line (— — —) is at $\tau=25\,000$ hartree^{-1}, the short-dashed line (- - -) is at $\tau=12\,500$ hartree^{-1}, and the dotted line (· · ·) is at $\tau=7500$ hartree^{-1}. Note the improving agreement between unguided and guided as the time step for the latter is reduced. The guided-walk energies follow the same trend, see Table II.

the probability density functions $p(r)$ at small particle separations (r) corresponding to several values of τ, with that of the unguided walk for He_3. Fluctuations in p indicate trapping in certain regions and lack of penetration into others. These fluctuations decrease as τ is reduced, resulting in convergence to the unguided probability density function and agreement in the computed energies.

It is important to point out that the error in the energy at the larger time steps is not systematic. The trapping of points, or conversely the inability to sample certain domains at small particle separation (for a practical amount of sampling), will result in energies either too high or too low, depending on the sign of the local energy at small r and whether p is too high or too low. For the same reasons, statistical error may be artificially high or low when obtaining an accurate representation of $p(r)$ at small r is problematic.

For purposes of comparing efficiency with the unguided walk, the statistical error in the energy per point sampled, σ, is presented in the last column of Table II. For M points, σ is equal to the statistical error in the average times $\sqrt{M}$. This statistic depends on the sampling inefficiency of the algorithm, i.e., the degree to which successively sampled points are correlated, as well as the nonconstancy of E_L, which is determined by the wave function. Since Ψ is the same for the computations on a given cluster, algorithm efficiency may be directly compared. Table II shows that while agreement with unguided energies is obtained by the guided walk at sufficiently small τ, the unguided walk is consistently more efficient, with σ an order of magnitude smaller, yielding a decrease in computational efficiency of two orders of magnitude. Correspondingly, for the guided walk at the smallest time step, the average step size ($\langle \Delta R \rangle$) is four to five times smaller than that for the unguided walk. Nevertheless the guided walk still gives good precision for reasonable computational effort. If this is also the case with the DMC approach, the increase in accuracy will be well worth the computational effort.

The guided-walk approach we have employed is inefficient because of the rapid increase in the guiding force as atoms coalesce. This suggests that a guided-walk approach with a better behaved force will not encounter the difficulties found here. We have investigated two such choices in a few selected applications. The first, "weighted unit force," approach simply employs $c\hat{\mathbf{F}}_i$ in place of $\mathbf{F}_i=\nabla_i \ln|\Psi|^2$ when moving particle i. Thus the direction of the original $\mathbf{F}$ is preserved while its magnitude c is held constant. In the second, a "damped force" approach, $\chi_i \mathbf{F}_i$ replaces $\mathbf{F}_i$, where

$$\chi_i = \exp\left[\sum_{j\ (\neq i)} t_2(r_{ij})\right], \tag{32}$$

and a_0 in t_2 becomes an adjustable parameter. Once again, the direction of the force is left unchanged but now its magnitude is most greatly affected only in the trapping regions, i.e., $|\chi_i \mathbf{F}_i| \to 0$ when $\Psi \to 0$.

For the H_2He test case the parameters governing the force, c and a_0, are varied together with τ to obtain maximum $\langle \Delta R \rangle$, which is roughly the same for the two guided walks. Trapping is not observed in either case and values of $\langle \Delta R \rangle$ are obtained which are a factor of 2 greater than the maximum obtainable in the unguided walk. However, the statistical error in the energy shows little variation among the unguided, weighted, and damped approaches. On the other hand, guided-walk statistical errors in both $\langle r \rangle$ and $r_{\rm rms}$ are about 25% lower than those of the unguided walk.

For the second test case, He_{112}, only the damped force approach was compared against the unguided walk. While exhibiting no trapping, the damped force walk yielded no increase in efficiency over the unguided walk. Therefore we conclude that the simple unguided walk is competitive with the guided-walk approaches studied here.

B. DMC Computations on helium clusters

For the DMC walks, inaccurate sampling at small r can have an effect significantly greater than that observed for the guided walk. If points are temporarily trapped in a region where the local energy is very low, as we have seen can easily occur at small r, the branching factor will be very large, resulting in a quickly increasing number of walkers at small r. Although the particles trapped at a small separation may move to larger r after a short period of time, the continuous generation of new walkers at this point will yield a high degree of oversampling and thereby a highly biased (too low) energy. Therefore, at a given time step, trapping may not be problematic for the guided walk but nevertheless gives instability in the DMC approach. So we expect that smaller time steps will be required to obtain convergence in the DMC walk than in the guided walk. This is investigated below.

Given the instabilities possible in DMC, we take two steps to monitor the behavior of the walk. First, we allow the ensemble to only reach twice (or four times for the larger clusters) its original size. If the maximum ensemble size is attained, this event is recorded and all weights are carried so that the copying of walkers is no longer employed. To some extent this step controls instabilities arising from trapping in that the continuous replication of trapped walkers is not permitted. Additionally, if the weight of any walker exceeds a given value (10), the weight is recorded in the output file.

Results for the energy and its growth estimate E_G are presented in Table III and plotted in Figs. 2(a)–2(c) for He_{3-5}. Block length, on the order of 10^5–10^6 hartree^{-1}, was varied by factors of 2–4 resulting in no significant change in the computed energies. Also, maximum ensemble sizes (200) and excessive weights (10), while found at the larger time steps, were not observed at the smaller (last two or three) values of τ. Given this, and the statistical agreement of the energies at the smaller time steps, the DMC energies we have computed are deemed to be well converged. However, we do see that much smaller values of τ are indeed required than was the case for the guided walk; approximate comparisons are 1000 versus 12 500 hartree^{-1} for He_3, 1500 versus 25 000 hartree^{-1} for He_4, and 1500 versus 10 000 hartree^{-1} for He_5 (compare Tables II and III).

Umrigar, Runge, and Nightingale have recently de-

TABLE III. DMC energy vs time step for He_{3-5}. The average of the local energy is E and the growth estimate is E_G. Time steps are given in hartree^{-1}, lengths are in Å, and energies are in K. AR denotes the acceptance ratio.

$10^{-3}\tau$	AR	$\langle \Delta R \rangle$	E/N	E_G/N
		He_3		
4.0	0.9963	0.62	−0.048 6(14)	−0.044 7(7)
3.0	0.9975	0.54	−0.046 2(7)	−0.044 28(35)
2.0	0.9986	0.44	−0.044 33(16)	−0.044 06(17)
1.0	0.9995	0.31	−0.044 09(18)	−0.043 98(17)
0.5	0.9998	0.22	−0.044 28(20)	−0.043 93(23)
		He_4		
5.0	0.9908	0.69	−0.175 0(90)	−0.145 5(7)
2.5	0.9965	0.49	−0.151 4(38)	−0.145 4(6)
2.0	0.9975	0.44	−0.148 1(16)	−0.145 7(7)
1.5	0.9983	0.38	−0.144 5(3)	−0.144 8(4)
1.0	0.9991	0.31	−0.144 5(3)	−0.144 4(3)
		He_5		
2.0	0.9963	0.45	−0.282(13)	−0.268 2(8)
1.5	0.9975	0.38	−0.268 3(5)	−0.267 5(4)
1.0	0.9986	0.31	−0.267 3(11)	−0.267 4(10)

scribed a DMC approach which controls the magnitude of **F** near its singularities and yields a better approximation to the Green's function in this domain [41]. It will be of interest to see if this method will reduce time-step bias, and thereby increase efficiency by allowing greater values of τ, in DMC computations on helium clusters.

Neglecting the different time-step scales, the behavior of the DMC energies is very similar to those of the guided walk. In essence, both walks are affected by trapping, which is magnified by the branching in the DMC walk. As was also the case for the guided walk, the coordinate expectation values, $\langle r \rangle$ and $R_{\rm rms}$, were not visibly affected by τ. This is not surprising as these quantities are only weakly influenced by sampling accuracy at small particle separations. This lack of time-step bias is also seen for the particle separation density functions $p(r)$ (except of course at small r), as well as for the density profiles.

Computational cost in obtaining converged DMC energies was large but not excessive. While He_3 presented an especially difficult case requiring five Cray X-MP14 CPU hours for all (not each) of the time steps, He_4 and He_5 took only one and two hours, respectively. As for H_2He at the VMC level of theory, the smallest and most diffuse cluster gave the greatest difficulty in obtaining the accuracy and precision desired.

Having successfully obtained converged energies for the smaller clusters, it was of interest to see if this could also be achieved for the larger clusters. We found for He_N, $N=7$, 14, 20, and 112, DMC energies converged at about $\tau=500-1500$ hartree^{-1}. Even at the largest time step of 2000 hartree^{-1}, the energies were very close to those computed at the smallest values of τ. Overall, the dependence of E/N and E_G/N versus the time step mimics that of the smaller clusters. At "larger" τ ($\approx$2000 hartree^{-1}), bias is noticeable and large weights and fluctuations in ensemble size occur. At "smaller" τ ($\approx$1000 hartree^{-1}), stability in the DMC energies, weights, and ensemble sizes is obtained. Therefore, while the required time step for unbiased energies is greatly reduced for DMC versus the guided walk, this is not the case for larger clusters versus smaller clusters. Unbiased energies are obtained at $\tau=1000-1500$ hartree^{-1} for 3–5 atoms and $\tau=500-1500$ hartree^{-1} for 7, 14, 20, and 112 atoms. (Here, absence of bias, i.e., it being masked by statistical error, is relative rather than absolute. For example, a bias of 0.005 K is very large for He_3, 11% of E/N, but on the order of the statistical error for H_{112}, 0.1% of E/N.) This is explained by the fact that convergence in DMC is most affected by trapping combined with large fluctuations in the local energy at small r—effects which are governed mostly by the wave-function form rather than by cluster size. Total computational cost was roughly 2, 4, 5, and 17 Cray X-MP14 CPU hours for $N=7$, 14, 20, and 112, respectively.

The DMC results are summarized and compared to GFMC [10,11] and other recent DMC results [18] (He_{20} and He_{112}) in Table IV. The results we compare against were obtained with the HFDHE2 potential [32] which predates the most recent, HFD-B(HE), potential [31] used here. The two potentials possess practically identical functional forms but with different sets of parameters. Perhaps most significant is the 1.3% increase in well depth. For the unit radius, $r_0 \equiv \sqrt{5/3} R_{\rm rms}/N^{1/3}$, we employ a "second-order" approximation of exact expectation values [7] defined as

$$\langle A \rangle_s \equiv 2\langle \Psi | A | \phi_0 \rangle / \langle \Psi | \phi_0 \rangle - \langle \Psi | A | \Psi \rangle , \qquad (33)$$

with $A = R^2$. Writing $\Psi = \phi_0 + \delta$ shows that $\langle A \rangle_s$ differs from the exact value, $\langle \phi_0 | A | \phi_0 \rangle$, by integrals involving δ^2. (This approximation is useful when A does not commute with the Hamiltonian. Methods for computing $\langle \phi_0 | A | \phi_0 \rangle$ have been described elsewhere [42,43].)

The DMC energies we compute with the HFD-B(HE) potential are significantly below the GFMC energies resulting from the previous, HFDHE2, potential. The relative discrepancies tend to decrease with increasing cluster size. For He_3 our energy is 13% lower than the GFMC value while for He_{14} and He_{20} the differences are only 3.3% and 3.7%, respectively. However, as seen in Table IV, for He_3 and He_{20} our DMC energies are in excellent agreement with GFMC when the same potential (HFDHE2) is employed. In contrast, our HFDHE2 energy does not agree with GFMC for He_{112}. The new potential lowers our He_{112} DMC energy by 3.2%. Such sensitivity to small changes in the potential has been observed previously. Kalos *et al.*, employing the HFDHE2 potential in their study of liquid ^4He, obtained a 6% decrease in the energy for a 1.9% increase in the well depth [44].

Upon considering He_{112} and comparing with the DMC energies computed by Chin and Krotscheck [18] (CK), employing a DMC algorithm different than our own [45], discrepancies not attributable to the potential arise. For He_{20}, we see in Table IV that CK's energy is 2% below both our DMC and the GFMC values, when all three calculations employ the same (HFDHE2) potential. For He_{112}, further disagreement occurs with the same potential as our and CK's energy lie roughly 2% and 3%, respectively, below GFMC. This is not readily explained by statistical error which, for both GFMC and DMC, is an order of magnitude smaller than these differences. It

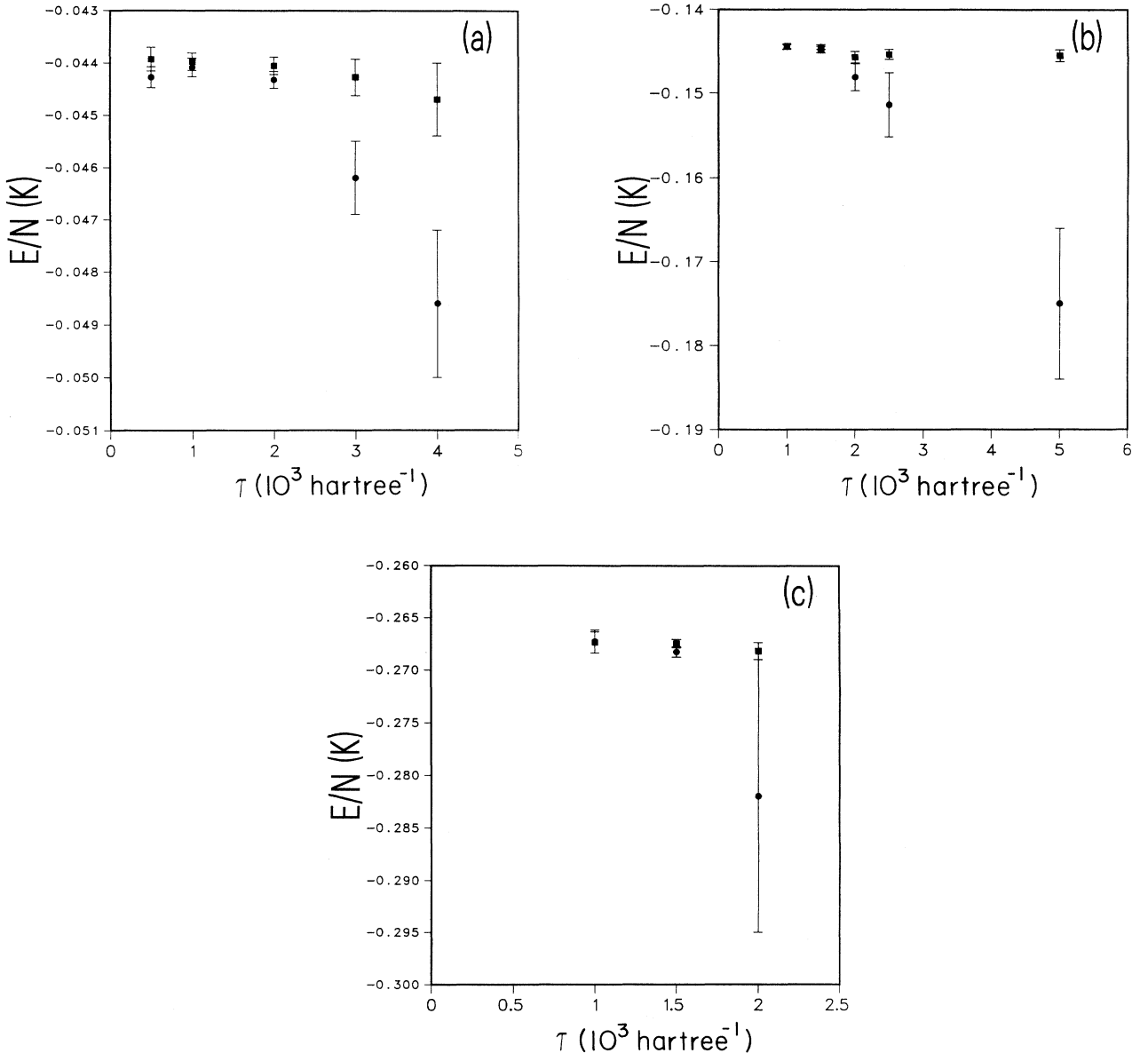

FIG. 2. Local (circles) and growth (squares) energy estimates of the exact energy vs τ for (a) He_3, (b) He_4, and (c) He_5.

TABLE IV. Comparison of GFMC and DMC energies and unit radii of helium clusters. Lengths are in Å and energies are in K.

Cluster	E/N	E_G/N	E_{GFMC}/N	r_0(DMC)	r_0(GFMC)[a]
He_3	−0.039 19(8)[b]	−0.039 07(13)[b]	−0.039 10(10)[a]	5.81[b]	5.35[a]
	−0.044 23(10)	−0.043 99(11)		5.59	
	−0.044 26(12)[c]	−0.044 21(11)[c]		5.60[c]	
He_4	−0.144 5(2)	−0.144 6(2)	−0.133 3(5)[a]	4.13	4.20[a]
He_5	−0.267 8(6)	−0.267 5(5)	−0.251 4(4)[d]	3.65	
He_7	−0.522 1(5)	−0.521 2(5)	−0.496 5(7)[d]	3.22	
He_{14}	−1.247 8(12)	−1.244 3(12)	−1.208 0(40)[d]	2.83	
He_{20}	−1.626(2)[b]	−1.621(3)[b]	−1.627(3)[d]	2.72[b]	2.71[a]
	−1.659(3)[e]			2.68[e]	
	−1.688(2)	−1.675(2)[f]		2.69	
		−1.689(5)[g]			
He_{112}	−3.664(3)[a]	−3.657(5)[b]	−3.600(10)[d]	2.40[b]	2.44[d]
	−3.726(4)[e]			2.42[e]	
	−3.780(3)	−3.773(5)		2.39	

[a]Reference [10].
[b]This work. DMC computed with the same potential, Ref. [32], as GFMC.
[c]Computed using a more highly optimized wave function.
[d]Reference [11].
[e]Reference [18]. DMC employing the potential of Ref. [32] and wave functions with three-body correlations.
[f]Computed with renormalization.
[g]Computed without renormalization.

is also not likely that wave-function quality is the cause. Our He_{20} wave function used for DMC possesses only two-body correlations and has a VMC energy which is 4% higher than that of CK, which includes three-body correlations. On the other hand, our He_{112} wave function, including three-body correlations as does that of CK, yields a VMC energy 1.4% below that of CK.

In spite of the above disagreements with previous GFMC and recent DMC energies, we feel that both our old- and new-potential DMC energies possess an accuracy well approximated by the statistical errors we report. For every cluster, a region of time-step sizes yielding stability in the energy is observed. Even for our largest cluster, He_{112}, computing at $\tau=1000$ and 500 hartree^{-1} gives a difference in E/N of only 0.05%, much less than the statistical error of 0.12% in each value, and weights and ensemble sizes are well behaved. In addition, we do obtain agreement with GFMC for $N=3$ and 20. These cluster sizes should not be problematic for GFMC despite the use of only two-body correlations in the wave function.

For He_{112}, none of the computed energies are in agreement and this deserves further comment. We point out that very slow convergence in GFMC, from a relatively simple starting function, was observed [10] for He_{112} and could give too high an energy in this case. Concerning CK's result, we note that they obtain an energy 2% below both GFMC and our DMC at $N=20$ where we expect GFMC to be more reliable. If CK's He_{20} energy is too low, then their He_{112} energy may be as well. On the other hand, CK have produced reasonable consistency in their computed energies when using different wave functions; differences are 0.5% and 0.6%, for He_{20} and He_{112}, respectively. They have also varied the time-step size.

As a final consideration, we compare the average local energy $\langle E_L \rangle$ and growth energy estimators E_G. While these estimators are highly correlated through their mutual dependence on the local energy, they often possess different time-step dependences, as is the case here [see Figs. 2(a)–2(c)]. Therefore convergence of these two estimators to statistically identical values also argues for the reliability, i.e., absence of time-step bias and thereby accuracy, of our computed DMC energies. In Table IV we see that agreement between both of our DMC energy estimates is excellent. The differences, for which the maximum is only 0.5% for He_3, are generally lower than the precision obtained. The largest discrepancy relative to statistical error occurs for He_{20}, $E_G/N=-1.6748(17)$ versus $E/N=-1.6879(16)$ K. This difference results primarily from computing $P(0)$ [see Eq. (13)] at the beginning of each block, directly after renormalization. (The final population is computed at the end of the block.) Thus, while the effect of renormalization is negligible for the block as a whole, its effect (especially on ensemble size) is greatest at the beginning of the block. We also performed calculations which omitted renormalization. (Although yielding larger fluctuations in ensemble size, the omission of renormalization was not problematic here.) While this had no effect on the local energy average (E/N), excellent agreement between E/N and E_G/N, −1.6879(16) versus −1.6885(46) K, was now obtained for He_{20}. The computation of $P(0)$ directly after renormalization most likely also accounts for the small (but beyond statistical error) difference between the two energy estimates for He_{14}. Since renormalization may often be desirable, a useful alternative is to compute $P(0)$ some time after renormalization, when the popula-

tion has equilibrated. This was done for He_3, reducing the discrepancy between the two energy estimates from 0.9% to 0.5%, thereby giving near statistical agreement.

For the unit radii r_0, we first compare our DMC and the GFMC values for He_3 and He_{20} computed using the same potential (Table IV). While agreement is observed for He_{20}, a large difference of 8% is seen for He_3. This difference is well beyond our statistical error of 1%. (Except for He_3, statistical error in DMC values of r_0 is well under 1%, i.e., 0.01–0.02 Å.) Furthermore, this disagreement with GFMC does not appear to be caused by error in our second-order estimate of r_0. The error in the second-order estimate of r_0, $\approx\langle\delta|R^2|\delta\rangle$, should be less than the difference between the VMC and DMC values, $\approx\langle\delta|R^2|\Psi\rangle$, which is only 2%. For the largest cluster, $N=112$, disagreement resurfaces when comparing our value of r_0 against GFMC obtained with the same potential. The difference between our VMC and DMC values is only 0.6%, implying an error of much less than 0.6% in the second-order estimate. Statistical error in the second-order values, 0.003 Å or less, cannot be the cause of the 2% discrepancy between second-order DMC and GFMC.

The unit radii computed by CK differ slightly from our own, 1.5% below for He_{20} and 0.8% above for He_{112}. These differences are most likely caused by the differences in the DMC solutions obtained, as reflected by the energies, rather than by the second-order approximation. This is supported by the fact that CK also obtain very good agreement between their VMC and second-order unit radii.

Finally, in comparing results using the HFD-B(HE) potential for He_{112}, we note that the difference between VMC and DMC is only 0.6%. Therefore, in this case, we

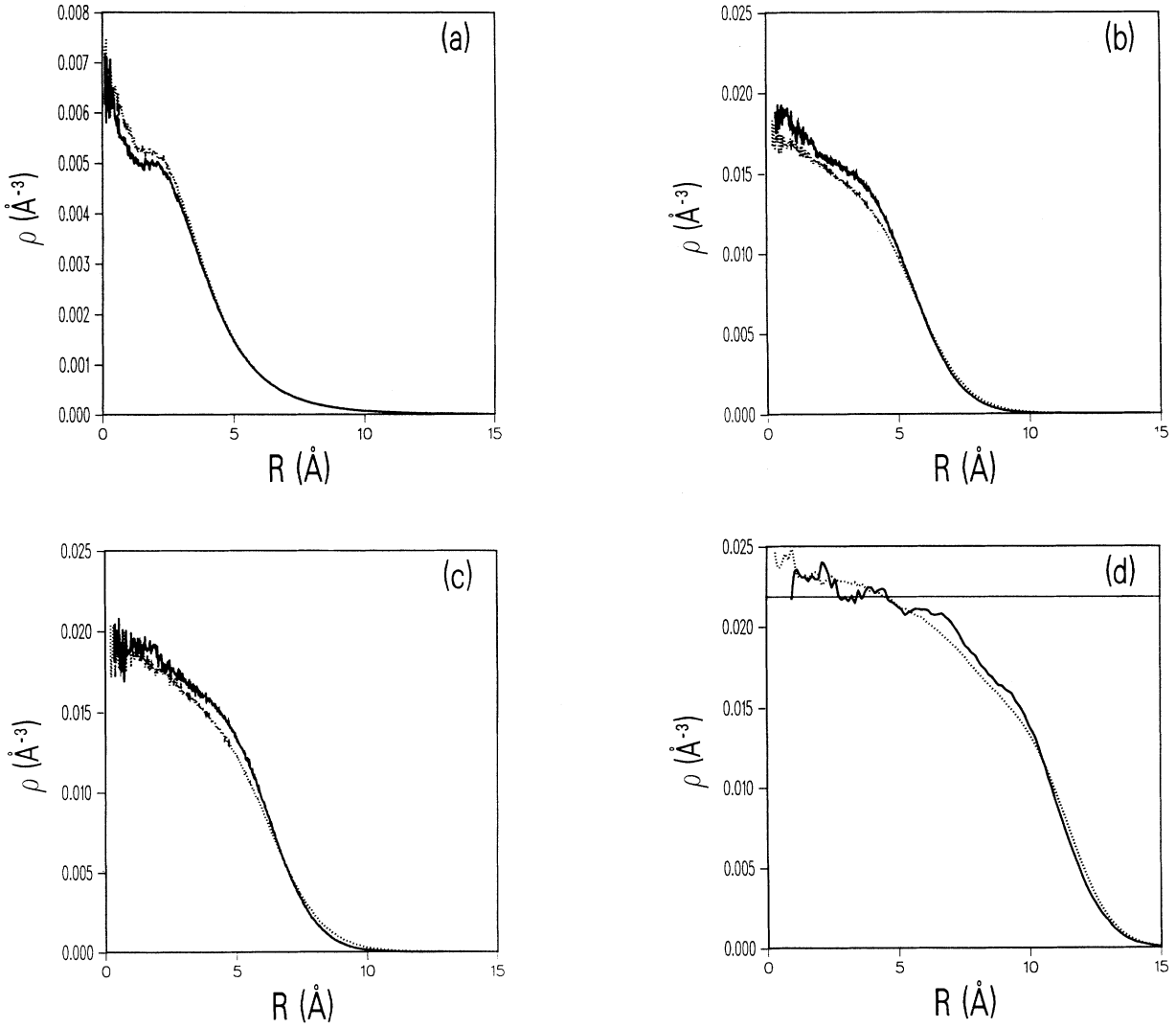

FIG. 3. VMC and second-order density profiles for (a) He_3, $\tau=500$ hartree^{-1}, (b) He_{14}, $\tau=500$ hartree^{-1}, (c) He_{20}, $\tau=750$ hartree^{-1}, and (d) He_{112}, $\tau=1000$ hartree^{-1}. The dotted line is the VMC and the solid line is the second-order approximation to the exact [Eq. (33)]. The straight line in (d) represents the experimental liquid-helium density of 0.021 85 Å^{-3}.

also expect our computed value of r_0 to be accurate to the number of figures shown. The change in r_0 on comparing the old- versus the new-potential values (2.396 versus 2.390 Å) is only 0.3%, significantly less than the 1% difference we find for He_{20}. In all cases where comparison is made, r_0 is reduced when employing the potential with the deeper well, as expected. This effect decreases by an order of magnitude, 3.8% to 0.3%, in passing from three to 112 atoms and contrasts with the change in the energy, 13.2% to 3.2%.

Of greater interest is the reliability of our reported estimates of r_0 obtained with the most up-to-date potential. We have found that the differences between VMC and DMC reach a maximum of only 3% (He_4 and He_7). Therefore we expect an accuracy of at least 3% in our estimates of r_0. However, the accuracy is probably much better; for He_3 0.5% agreement is obtained from wave functions with noticeably different VMC values of r_0, 5.50 and 5.74 Å, i.e., above *and* below the estimated exact value.

Figures 3(a)–3(c) present VMC and second-order ($\tau=500-1000$ hartree^{-1}) [see Eq. (33)] density profiles for He_3, He_{14}, and He_{20}. The bin sizes are very small, 0.026 Å for He_3 and 0.019 Å for He_{14} and He_{20}. This allows for very fine detail in ρ, and although there is enhanced statistical error near the origin, it remains below 10% down to about 0.2–1 Å. We see for these clusters, as well as for the other clusters not shown, that

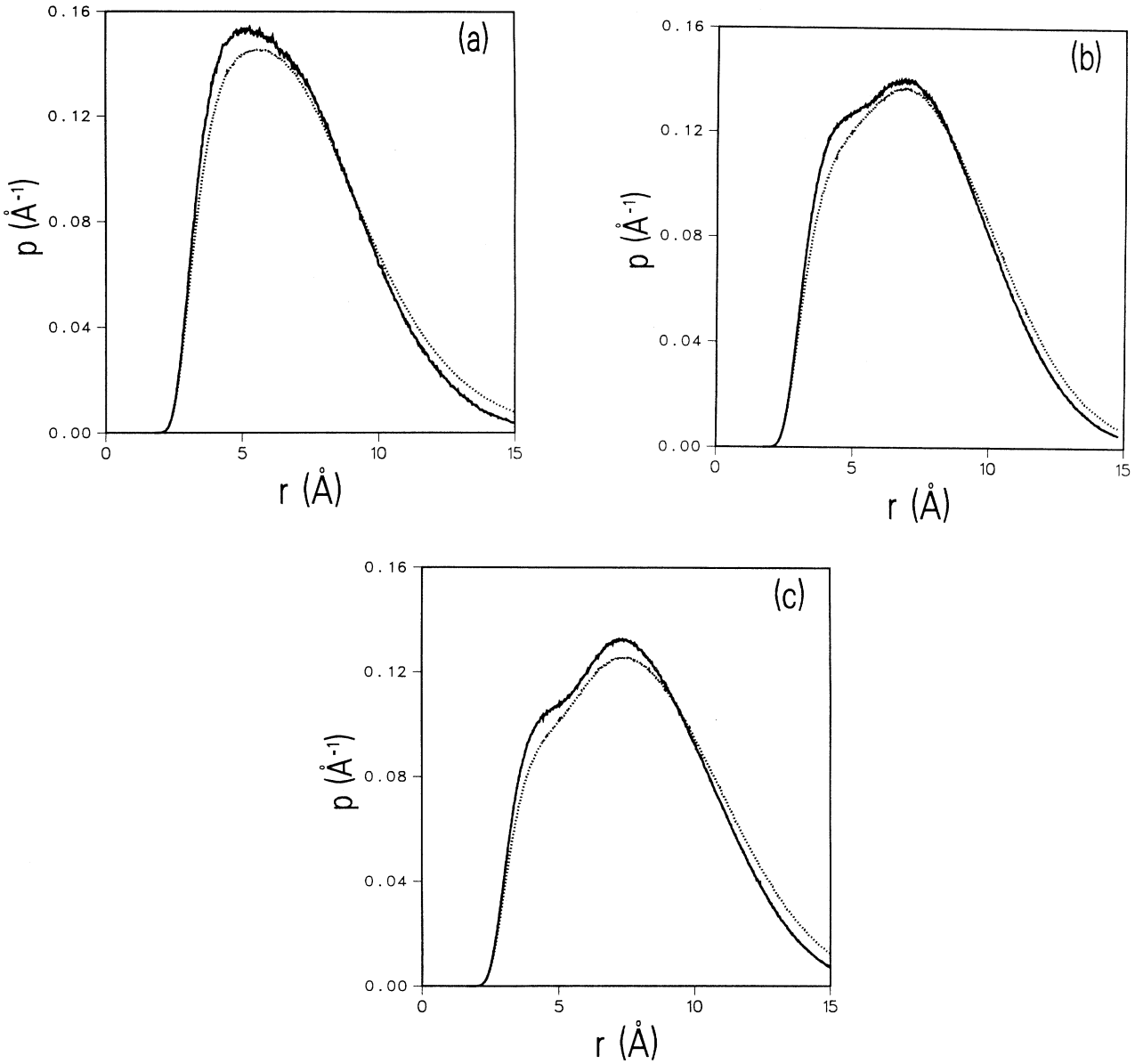

FIG. 4. VMC and second-order probability density functions of particle separation for (a) He_7, $\tau=500$ hartree^{-1}, (b) He_{14}, $\tau=500$ hartree^{-1}, and (c) He_{20}, $\tau=750$ hartree^{-1}. The dotted line is the VMC and the solid line is the second-order approximation to the exact.

the qualitative behavior is unchanged between the VMC and second-order profiles. The sharp increase in ρ near the cluster center for He_3, which we first observed at the VMC level of accuracy and which arises from a significant contribution of near-collinear configurations to the density [28], remains in DMC. For 14- and 20-atom clusters, very little structure is evident. The He_{14} density rises slightly near the origin while that of He_{20} reaches a constant value at about 2.5 Å and then fluctuates about 0.019 $Å^{-3}$. This is in good agreement with GFMC [10] and the oscillations seen by CK are not observed here.

VMC and second-order ($\tau=500$ $hartree^{-1}$) density profiles for He_{112} are computed with a bin size of 0.13 Å and are presented in Fig. 3(d). The experimental liquid-helium density of 0.021 85 $Å^{-3}$ is shown for comparison as a solid line. Statistical error is 10% for the points nearest the origin, then decreases rapidly at greater distances, and finally begins to rise near the cluster edge, reaching about 10% at 11 Å. Unlike any of the smaller clusters, structure in the density profile now appears to be present. However, further analysis indicates that the fluctuations at $R<5$ Å are statistical. Only in a very small region, 2.10–2.35 Å, is statistical error (4.5%) significantly below the deviation from the liquid density (6%–10%). Thus, out to 4.8 Å, the density is very nearly constant to within reasonable statistical error (under 5% for $R>1.5$ Å). However, a shoulder is present at 6.2 Å where statistical error is very small, 1.5%. Further out, another shoulder at 9.6 Å is barely discernible. This is in good agreement with CK (bin size is 0.24 Å), who also observe shoulders in these regions. We have also computed a second-order density profile for He_{112} employing the HFDHE2 potential. The results are very similar to those we obtained above.

In summary, our second-order densities for $N=14$, 20, and 112 rise up to their central values at some distance from the origin. The value of this central density and the distance to which it extends increases with cluster size. The He_{14} central density is clearly below that of liquid helium and ρ begins to drop off at about 1 Å. That of He_{112} is in good agreement with the liquid-He density and extends out to about 4.5 Å while the He_{20} case is intermediate between He_{14} and He_{112}. These conclusions differ from those of CK, who obtain oscillations in their density profiles as the origin is approached for both He_{20} and He_{112}. We see no such oscillations for He_{20} while those of He_{112} are mostly removed upon considering the small (2%–5%) statistical error. However, we do see shoulders in the He_{112} density at larger R.

For all clusters, the quantitative differences between the VMC and second-order density profiles are not large. The small changes we observe in passing from VMC to second order lead us to believe our estimate of exact density profiles by second-order profiles is well justified (see discussion concerning the unit radii). Comparison against density profiles computed by VMC [26] or GFMC [10] shows little variation in the central density, despite the different potentials and wave functions employed. A major difference does arise for He_3 which has a sharp increase in ρ at about 2 Å [28] which is not evident in GFMC [10].

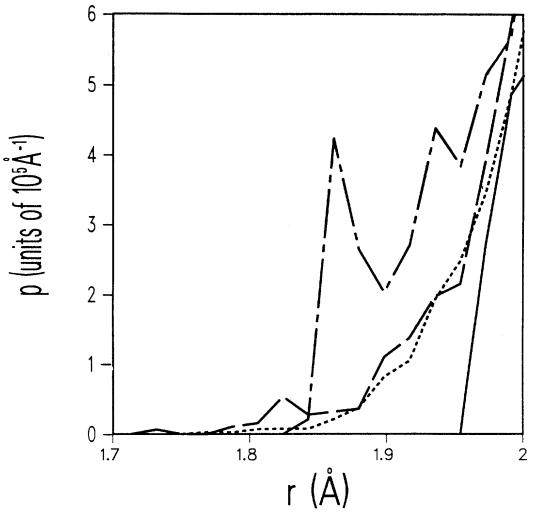

FIG. 5. VMC (——) and DMC plots of $p(r)$ at short range for He_{14} at $\tau=2000$ (—·—·), 1000 (— — —), and 500 (· · ·) $hartree^{-1}$.

In order to gain further insight into cluster structure and its changes as accuracy is improved from VMC to the second-order approximation, we compute particle separation probability density functions $p(r)$. Figures 4(a)–4(c) present VMC and second-order plots of $p(r)$ for He_7, He_{14}, and He_{20}. For He_{3-5}, qualitative distinctions are not discernible between the VMC and second-order density functions, just as for He_7. For those clusters which show structure in p with VMC, He_{14} and He_{20}, qualitative differences between VMC and second-order densities are now apparent. We see that the implied shoulder in p found by VMC becomes much more pronounced as we progress to the second-order level of accuracy. It would be interesting to see if this onset of "shell" structure is progressive or abrupt as cluster size is increased from 7 to 14 atoms. We point out once more that both ρ and p are essentially independent of the time step employed (for the range of τ we have considered). The exception of course is for p at small r. An example of this is given in Fig. 5 which presents the VMC and several second-order estimates in the region $p(r)/p_{\max}<5\times10^{-4}$ for He_{14}. Note that by $\tau=1000$ $hartree^{-1}$ convergence is quite good, as is the case for the energy. (See Table IV and associated discussion.)

C. New two-body form and T_3

We have employed our new two-body form, t_2' [see Eq. (24)], in unguided-walk computations on He_N, $N=3$, 7, and 20. For each cluster the same value of Δ is employed for t_2 and t_2'. We find that t_2 yields the best energy for He_3, 5% below that of t_2'. However, for the larger clusters, small but significant (i.e., well beyond statistical error) reductions are obtained with t_2', i.e., 2% for He_7 and 1% for He_{20}. For He_3, the most diffuse cluster, the re-

duced flexibility of t_2' in describing long-range behavior is significant. In addition to yielding a poorer energy, t_2' also gives an unrealistically low unit radius. For the more tightly bound clusters, for which short-range interactions are more important, an improvement with t_2' is obtained. Also, t_2' yields a 30% reduction in statistical error in the energy, even for He_3, presumably by better describing the short-range behavior where the local energy possesses its greatest fluctuations. Consequently, we expect that further accuracy may be obtainable by increasing the long-range flexibility of t_2'.

In addition to seeking better two-body wave functions, accuracy can also be increased by including three-body (and higher) effects, as discussed in Sec. IV A. We treat here the larger clusters, whose wave functions should possess the greatest need for three-body correlations. For He_{14} and He_{20}, the initial parameters in T_2 (t_2 here) are obtained from a conjugate-gradient optimization. For He_{112} initial parameters are those for He_{20} and are then varied by hand. As seen in Table I, optimization resulted from changing only the long-range parameters. Upon addition of T_3, parameters are varied by hand in a set of short Monte Carlo runs. At this stage, only variation of the T_3 parameters and of the long-range parameters in T_2 was found to be fruitful. Despite the approximate level of optimization, a significant reduction in the energy is observed in all cases. The optimized T_3 term yielded about a 6% improvement in the energy for He_{14} and He_{20}. As expected, the He_{112} energy is reduced by a greater amount (9%) than for the smaller clusters. The final result is that the VMC energies of the $N=14$, 20, and 112 clusters are quite good; 96.1% of the computed exact value is obtained for He_{14} and this decreases only by 1.5% upon going to He_{112}.

Wave-function quality is also improved in other respects. The data listed in the middle of Table V show that the *relative* statistical error in the energy decreases in every case. The increased computation when T_3 is in the wave function ranges from 82% for He_{14} to 88% for He_{112}. Allowing for this, the efficiency (the inverse product of the variance and the computation time) in computing the energy is increased by a factor of 2 for He_{14} and He_{112}. Interestingly, however, efficiency is decreased by 19% for He_{20}. This contrast with the He_{14} and He_{112} cases may arise from incomplete (hand) parameter optimization or from use of the energy, rather than variance, minimization criterion. It could also be magnified by the generally large uncertainties in computed statistical error.

TABLE V. Accuracies and precisions for two- and three-body wave functions.

	Accuracy in E/N (%)		$\sigma(E/N)/(E/N)$		Accuracy in r_0 (%)	
N	T_2	T_2+T_3	T_2	T_2+T_3	T_2	T_2+T_3
14	90.5	96.1	1.00	0.52	3.2	1.2
20	89.5	95.3	0.93	0.76	4.7	2.8
112	85.7	94.6	0.23	0.11	4.9	1.2

In the last two columns of Table V, percent differences between VMC and second-order unit radii r_0 are listed for the T_2 and T_2+T_3 wave functions of He_{14}, He_{20}, and He_{112}. We expect these differences to be good estimates of the deviation from exact values, given our confidence in the accuracy of our second-order estimates of r_0, see Sec. V B. In each case agreement with second-order estimates of r_0 is noticeably enhanced upon addition of the three-body correlation functions. The result is that very good agreement ($\approx 1\%$) with estimated exact unit radii is obtained at the VMC level of theory with the three-body wave functions. The exception is again He_{20} with a VMC value of r_0 differing by 3% from the second-order estimate.

VI. CONCLUSIONS

We have studied wave-function forms and Monte Carlo integration techniques for H_2He and He_N, $N=3-20,112$. As a very diffuse system with a highly repulsive potential, H_2He presented special difficulties for the VMC computations. While the VMC approaches used here are without bias, errors in computed quantities can arise for a finite (yet large) amount of sampling if efficiency is sufficiently poor. Therefore only for very large attempted displacement sizes Δ is good accuracy obtained in the unguided walk. Furthermore, these values of Δ correspond to acceptance ratios of 0.35–0.40, well below the often assumed optimum of 0.5.

Despite the increased dimensionality in comparison to H_2He ($3N$ versus 3), the less diffuse helium clusters are much more amenable to Monte Carlo integration. For the unguided walk, consistency in computed expectation values is obtained over a wide range of Δ. However, we do find that statistical error in both $\langle r \rangle$ and in $R_{\rm rms}$ is noticeably lower at large Δ. Once again, these values of Δ corresponded to the largest average displacement of an attempted move, $\langle \Delta R \rangle$, rather than to an acceptance ratio of 0.5.

Directly including importance sampling by using a walk guided by $\mathbf{F}=\nabla|\Psi|^2$ yielded inaccurate H_2He energies. Although most of configuration space was well sampled, as indicated by accurate values of $\langle r \rangle$ and $r_{\rm rms}$, large values of the force $\mathbf{F}$ caused trapping at small r. The resulting inaccuracy in the density gave rise to significant errors in the computed energy because, although the wave function is small, the large magnitude of the local energy at small separations requires accurate sampling in this region. However, trapping is readily circumvented by employing a better behaved force. Two such approaches, which still direct moves toward a local maximum in $|\Psi|^2$, were applied to H_2He and He_{112}. Compared to an unguided walk, efficiency was increased slightly for H_2He but not for He_{112}.

As seen for H_2He, errors in the energy arise in a walk guided by $\mathbf{F}=\nabla \ln|\Psi|^2$ due to poor convergence at small r (which is practically infinitely long unless τ is very small). In light of the desire to compute exact energies by DMC, however, it was of interest to determine the domain of τ at which high accuracy could be obtained by this guided walk. We find that, though initially quite

poor at large τ, accurate energies are obtained at smaller values. "Convergence" in the guided-walk energies is directly correlated, as expected, with improving accuracy in $p(r)$ at small r as the time step is reduced. This was also the case in the DMC calculations, demonstrating that accuracy in the (DMC or VMC) energy is critically dependent on the sampling at small r. In light of this discussion, we point out that a DMC approach similar to that employed here but which bounds the magnitude of $\mathbf{F}$ near $\Psi=0$ has been described recently [41] and may be of use for the systems studied here.

Although small time steps are required, well-converged DMC energies have been obtained for He_N, $N=3-5,7,14,20,112$. The steps taken to ascertain convergence, variation of the time step and block size, comparison of the local and growth energy estimates, and convergence of p at small r, all support the reliability of the computed energies. As we have already found with VMC for He_3 and He_4 [28], energies well below those of GFMC [10,11] are obtained. For He_3 and He_{20}, these discrepancies are clearly caused by the use of different potentials. It is reasonable to conclude that this is also the case for all the 3–20 atom clusters studied here. The agreement we obtain with GFMC for an identical potential leads us to believe in the reliability of our DMC approach and the exactness of our computed energies with the most up-to-date potential. However, energies below GFMC (but with the same potential) have been obtained by CK using a modified DMC approach for He_N, $N=20$, 40, 70, and 112 [18], and by us for $N=112$. While the discrepancy between DMC and GFMC is smaller in our calculation than in CK's, our energy is still significantly lower than the GFMC result. Further disagreement occurs when comparing our DMC energies with those of CK. For both $N=20$ and 112, we compute slightly higher energies.

We see a sizable lowering of the energy below that obtained from the earlier, HFDHE2, potential when employing the most recent, HFD-B(HE), He-He interaction potential, 13% for three atoms and 3.2% for 112. This reflects primarily the lower well depth of the newer potential. Decreases in the unit radius are also observed, 3.8% for He_3 to 0.3% for He_{112}. Finally, as do CK, we see fluctuations in the He_{112} density profile which have not previously been observed at either the VMC or GFMC level of theory. However, our fluctuations at small R are beneath statistical error as differences from the liquid-helium density are generally less than one standard deviation in this region, $R<5$ Å.

In an effort to improve accuracy at the two-body level, we have studied an entirely new form describing these effects. This form gives added emphasis at small r and contains a factor which mimics the potential in this domain. Optimized wave functions for He_7 and He_{20} gave slightly improved energies, despite the reduced flexibility at large r. For the more diffuse He_3, the older form gave a lower energy. In addition, statistical error in the energy was reduced by about a third. It is expected that a better description of the long-range behavior will yield further improvements.

In order to investigate the accuracy obtainable by current VMC approaches, a three-body factor was added to the 14-, 20-, and 112-atom two-body wave functions. Substantial improvement in the energy is obtained, and for He_{14} and He_{112} an increased efficiency in computing this quantity also results, despite the greater complexity of the wave function. More sophisticated optimization algorithms for the parameters in T_3 may yield a further lowering of the VMC energy. It also remains to be seen whether t_2', combined with T_3, will yield better agreement with exact energies, and whether the use of such complex wave functions will be advantageous for DMC.

ACKNOWLEDGMENTS

This work was supported by the Office of Naval Research under Grant No. N00014-89-J-1755, and by the National Science Foundation (Grant No. CHE-8907423). Acknowledgment is also made to the Donors of the Petroleum Research Fund, administered by the American Chemical Society, for partial support of this research. K.B.W. would also like to thank the Alfred P. Sloan Foundation for financial support.

[1] For an up-to-date review, see Proceedings of the Fifth International Meeting on Small Particles and Inorganic Clusters, Konstanz, Federal Republic of Germany, 1990 [Z. Phys. D **19** (1991); **20** (1991)].

[2] N. Metropolis, A. W. Rosenbluth, M. N. Rosenbluth, A. H. Teller, and E. Teller, J. Chem. Phys. **21**, 1087 (1953).

[3] M. H. Kalos and P. A. Whitlock, *Monte Carlo Methods* (Wiley, New York, 1986), Vol. 1, Chap. 3.

[4] G. E. P. Box and M. E. Mueller, Ann. Math. Stat. **29**, 610 (1958).

[5] M. H. Kalos, J. Comput. Phys. **1**, 257 (1966).

[6] M. H. Kalos, D. Levesque, and L. Verlet, Phys. Rev. A **9**, 2178 (1974).

[7] P. A. Whitlock, D. M. Ceperley, G. V. Chester, and M. H. Kalos, Phys. Rev. B **19**, 5598 (1979).

[8] D. M. Ceperley and B. J. Alder, J. Chem. Phys. **81**, 5833 (1984).

[9] K. E. Schmidt and J. W. Moskowitz, J. Stat. Phys. **43**, 1027 (1986).

[10] V. R. Pandharipande, J. G. Zabolitzky, S. C. Pieper, R. B. Wiringa, and W. Helmbrecht, Phys. Rev. Lett. **50**, 1676 (1983).

[11] R. Melzer and J. G. Zabolitzky, J. Phys. A **17**, L565 (1984).

[12] J. G. Zabolitzky, in *Progress in Particle and Nuclear Physics,* edited by A. Faessler (Oxford, New York, 1986), Vol. 16, p. 103.

[13] J. B. Anderson, J. Chem. Phys. **63**, 1499 (1975).

[14] D. R. Garmer and J. B. Anderson, J. Chem. Phys. **86**, 4025 (1987); **86**, 7327 (1987).

[15] P. J. Reynolds, D. M. Ceperley, B. J. Alder, and W. A. Lester, Jr., J. Chem. Phys. **77**, 5593 (1982).

[16] R. N. Barnett, P. J. Reynolds, and W. A. Lester, Jr., J. Chem. Phys. **77**, 4992 (1986).

[17] B. L. Hammond, M. M. Soto, R. N. Barnett, and W. A. Lester, Jr., J. Mol. Struct. **234**, 525 (1991).
[18] S. A. Chin and E. Krotscheck, Phys. Rev. B **45**, 852 (1992).
[19] H. Sun and R. O. Watts, J. Chem. Phys. **92**, 603 (1990).
[20] M. A. Suhm and R. O. Watts, Phys. Rep. **204**, 293 (1991).
[21] S. M. Rothstein and J. Vrbik, J. Chem. Phys. **87**, 1902 (1987).
[22] J. B. Anderson and D. R. Garmer, J. Chem. Phys. **87**, 1903 (1987).
[23] P. J. Reynolds, R. K. Owen, and W. A. Lester, Jr., J. Chem. Phys. **87**, 1905 (1987).
[24] R. N. Barnett, Ph.D. thesis, University of California, Berkeley, 1989 (unpublished).
[25] D. M. Ceperley, J. Comput. Phys. **51**, 404 (1983).
[26] V. R. Pandharipande, S. C. Pieper, and R. B. Wiringa, Phys. Rev. B **34**, 4571 (1986).
[27] M. V. Rama Krishna and K. B. Whaley, J. Chem. Phys. **93**, 6738 (1990).
[28] R. N. Barnett and K. B. Whaley, J. Chem. Phys. **96**, 2953 (1992).
[29] W. C. Meyer, P. C. Hariharan, and W. Kutzelnigg, J. Chem. Phys. **73**, 1880 (1980).
[30] G. Schatz (private communication).
[31] R. A. Aziz, F. R. W. McCourt, and C. C. K. Wong, Mol. Phys. **61**, 1487 (1987).
[32] R. A. Aziz, V. P. S. Nain, J. S. Carley, W. L. Taylor, and G. T. McConville, J. Chem. Phys. **70**, 4330 (1979).
[33] C.-W. Woo, Phys. Rev. Lett. **28**, 1442 (1972).
[34] C. C. Chang and C. E. Campbell, Phys. Rev. B **15**, 4238 (1977).
[35] V. R. Pandharipande, Phys. Rev. **B 18**, 218 (1978).
[36] K. Schmidt, M. H. Kalos, M. A. Lee, and G. V. Chester, Phys. Rev. Lett. **45**, 573 (1980).
[37] Q. N. Usmani, S. Fantoni, and V. R. Pandharipande, Phys. Rev. B **26**, 6123 (1982).
[38] The particular representation of T_3 given in Eqs. (27) and (28) is due to a private communication with S. C. Pieper.
[39] For an excellent description, see W. H. Press, B. P. Flannery, S. A. Teukolsky, and W. T. Vetterling, *Numerical Recipes* (Cambridge University Press, Cambridge, England, 1986), pp. 301–306.
[40] C. J. Umrigar, K. G. Wilson, and J. W. Wilkins, Phys. Rev. Lett. **60**, 1719 (1988).
[41] C. J. Umrigar, K. J. Runge, and M. P. Nightingale, in *Monte Carlo Methods in Theoretical Physics,* edited by S. Caracciolo and A. Fabrocini (ETS Editrice, Pisa, 1991), p. 161.
[42] K. S. Liu, M. H. Kalos, and G. V. Chester, Phys. Rev. A **10**, 303 (1974).
[43] R. N. Barnett, P. J. Reynolds, and W. A. Lester Jr., J. Comput. Phys. **96**, 258 (1991).
[44] M. H. Kalos, M. A. Lee, P. A. Whitlock, and G. V. Chester, Phys. Rev. B **24**, 115 (1981).
[45] S. A. Chin, Phys. Rev. A **42**, 6991 (1990).